Structural Polymorphism and Endotoxic Activity of Synthetic Phospholipid-like Amphiphiles†

K. Brandenburg,*,‡ L. Hawkins,§ P. Garidel,⊥ J. Andrä,‡ M. Müller,‡ H. Heine,‡ M. H. J. Koch,|| and U. Seydel‡

Forschungszentrum Borstel, Leibniz-Institut für Medizin und Biowissenschaften, Parkallee 10, D-23845 Borstel, Germany, and Department of Medicinal Chemistry, Eisai Research Institute, 4 Corporate Drive, Andover, Massachusetts 01810-2441, USA, and Institut für Physikalische Chemie, Martin-Luther-Universität Halle-Wittenberg, Mühlpforte 1, D-06108 Halle/Saale, Germany, and European Molecular Biology Laboratory, EMBL c/o DESY, Notkestrasse 85, D-22603 Hamburg, Germany

Received November 25, 2003; Revised Manuscript Received February 6, 2004

ABSTRACT: The physicochemical characteristics and in vitro biological activity of various synthetic hexaacyl phospholipid dimers were compared with the respective behavior of bacterial endotoxins (lipopolysaccharide, LPS). The structural variations of the synthetic amphiphiles include different stereochemical (*R*,*S*) configurations about their ester- and amide-linkages for the acyl chains and differences in the length of the serine backbone spacer. The temperature of the gel to liquid crystalline phase transition of the acyl chains (T_c) lies between 10 and 15 °C for the compounds with the shortest backbone and decreases rapidly for the compounds with longer backbones. The phase transition enthalpies (8−16 kJ·mol^{-1}) are considerably lower than those of lipid A from hexaacyl endotoxins (28−35 kJ·mol^{-1}). In contrast, the dependence of T_c on Mg^{2+} and water content shows a behavior typical for endotoxins: a significant increase with increasing Mg^{2+} and decreasing water concentrations. The aggregate structure is sensitively dependent not only on the length of the backbone spacer but also on the different stereochemical variations. It can be directly correlated with the biological activity of the compounds. Thus, as with natural lipid A, the capacity to induce cytokine production in mononuclear cells is directly related to the affinity to form nonlamellar cubic or inverted hexagonal H_{II} aggregate structures. Together with the data on the transport and intercalation of the dimers into phospholipid liposomes mediated by the lipopolysaccharide-binding protein (LBP), our conformational concept of endotoxicity and cell activation can be applied to these non-LPS structures: endotoxically active compounds incorporate into membranes of immune cells and cause conformational changes at the site of signaling proteins such as Toll-like receptors or K^+-channels due to their conical molecular shape.

Lipopolysaccharides (LPS), the endotoxins of Gram-negative bacteria, form the outer leaflet of their outer membrane. During cell division or upon attack of the immune system or destruction by antimicrobial drugs, LPS may be released from the bacteria into the blood circulation where it has been observed to induce a variety of biological effects in mammals such as fever, pyrogenicity, and septic shock (*1*). Chemically, it consists of an oligo- or polysaccharide chain covalently linked to a hexaacylated bisphosphorylated lipid moiety termed lipid A, which has been shown to represent the "endotoxic principle" of LPS (*2*). However, only relatively slight changes of the chemical structure, such as a reduction of the number of charges or the number and distribution of fatty acids or both, causes dramatic decreases of the bioactivity down to a complete loss of endotoxicity (*3*, *4*). The systematic investigation of the structural requirements for endotoxicity with synthetic lipid A analogues and partial structures exhibited a broad pattern of biological activities ranging from high endotoxicity for the synthetic analogue of natural hexaacyl lipid A from *Escherichia coli* to complete inactivity for tetraacyl lipid A precursor Ia or IVa (*5*, *6*). The latter, however, was able to inhibit the action of agonistical LPS, that is, to act antagonistically.

Aggregates of LPS and lipid A rather than monomers (*7*, *8*) are the biologically relevant units, which are required by binding structures in serum and on the cell surface in the very early steps of cell activation. Agonistically active lipid A of enterobacterial LPS adopts a cubic inverted structure under near physiological conditions, from which a conical shape of the individual lipid A molecule was deduced (*4*). In contrast, multilamellar aggregate structures were observed for agonistically inactive but antagonistic lipid A (*4*). A further precondition for agonism as well as for antagonism is the presence of two negative charges at the lipid A backbone, which is usually fulfilled by the two phosphates in 1 and 4′ positions of the diglucosamine backbone.

† Supported by Deutsche Forschungsgemeinschaft (Grant SFB 367, Project B8) and European Union (Project ANEPID). This study has been carried out with financial support from the Commission of the European Communities, specific RTD program "Quality of Life and Management of Living Resources", Grant QLK2-CT-2002-01001, "Antimicrobial endotoxin-neutralizing peptides to combat infectious diseases".

* Corresponding author. Forschungszentrum Borstel, LG Biophysik, Parkallee 10, D-23845 Borstel, Germany. E-mail: Kbranden@fz-borstel.de.

‡ Leibniz-Institut für Medizin und Biowissenschaften.

§ Eisai Research Institute.

⊥ Martin-Luther-Universität Halle-Wittenberg.

|| European Molecular Biology Laboratory.

10.1021/bi0361158 CCC: $27.50
Published on Web 03/06/2004

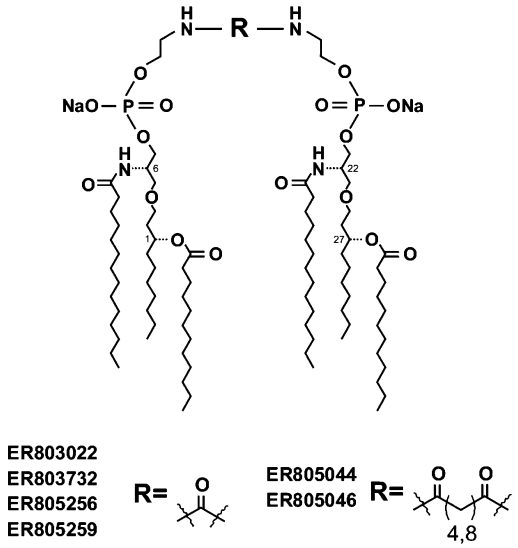

Compd. ER-	Stereochemistry *1,6,22,27*
803022	*R,R,R,R*
803732	*R,S,S,R*
805256	*R,R,S,S*
805259	*S,S,S,S*

Compd. ER-	*n*
805044	4
805046	8

FIGURE 1: Chemical structures of the six ER compounds. The compounds with larger backbone (ER805044 and ER805046) are in the stereochemical R,R,R,R configuration.

From these considerations, any amphiphilic molecules with negative charges in the hydrophilic backbone and clearly separated hydrophilic and hydrophobic moieties are candidates for agonistic or antagonistic endotoxin-like action, depending on whether they preferentially adopt a conical or a cylindrical shape, respectively. On this basis we have recently defined a "generalized endotoxic principle" by designing a synthetic phospholipid with an invariable hydrophobic moiety composed of six acyl chains symmetrically ester- or amide-linked to two phosphates, which are connected via a serine-like structure (compound ER803022) (*9*). We have shown that this compound fulfils all criteria of endotoxicity except for activity in the *Limulus* amebocyte lysate test, which recognizes the diphosphorylated diglucosamine backbone of lipid A (*10*). We have extended these investigations by synthesizing derivatives of compound ER803022 differing in the length of the linkage between the phosphates on the one side and the stereochemistry of the amide- and ester-linked acyl chains on the other side (Figure 1) and have found that the broad pattern of endotoxic action between highly active and inactive compounds can be mimicked by these synthetic phospholipids.

MATERIALS AND METHODS

Synthesis. The phospholipid-like structures ER803022, ER805044, ER805046, ER805256, ER805259, and ER803732 (chemical structures in Figure 1) were synthesized at EISAI Research Institute of Boston, Andover, MA, based on synthetic work done by Krisovitch and Regen (*11*). The preparation for the compounds are published as a U.S. Patent (*12*), and can be made available on request. The structures were confirmed by ^{1}H-, ^{13}C-, and ^{31}P NMR, mass spectrometry, and elemental analysis.

FTIR Spectroscopy. The infrared spectroscopic measurements were performed on an IFS-55 spectrometer (Bruker, Karlsruhe, Germany). For phase transition measurements, the lipid samples were placed in a CaF_2 cuvette with a 12.5 μm Teflon spacer. Temperature scans were performed automatically between 10 and 70 °C with a heating rate of 0.6 °C·min^{-1}. For measurement of hydrated lipid samples, these were spread on a ATR Ge plate, and free water was evaporated. Every 3 °C, 50 interferograms were accumulated, apodized, Fourier transformed, and converted to absorbance spectra.

Differential Scanning Calorimetry (DSC). DSC measurements were performed on a Perkin-Elmer Pyris-1 DSC (Norwalk, CT) with heating and cooling rates of 1 °C·min^{-1} in the temperature interval between −8 and 60 °C (*13*). The reproducibility was controlled in three consecutive heating and cooling scans (*14*). The accuracy of the DSC experiments was ±0.5 °C for the phase transition temperatures and ±1 kJ·mol^{-1} for the phase transition enthalpy. The DSC samples were prepared by adding 6 μL of buffer (phosphate buffer, pH 6.8) to DSC Al-pans (Perkin-Elmer, no. 219-0041) containing a known amount (~3 mg) of dry lipid powder. The pans were sealed and equilibrated for 2 h at −10 °C in the DSC instrument. The DSC data were analyzed using the Perkin-Elmer Thermal Data Analysis software. The phase transition enthalpy was obtained by integrating the area under the heat capacity curve (*14*).

X-ray Diffraction. X-ray diffraction experiments on the aggregate structures of the lipids were performed at the European Molecular Biology Laboratory (EMBL) outstation at the Hamburg synchrotron radiation facility HASYLAB using the double-focusing monochromator-mirror camera X33 (*15*). X-ray diffraction patterns, obtained with exposure times of 2 min using a linear gas proportional detector with delay line readout (*16*), were evaluated according to previously described procedures (*17*). These allow us to assign the spacing ratios to defined three-dimensional aggregate structures, from which the conformation of the individual molecules are deduced. In the diffraction patterns presented here, the logarithm of the scattering intensity, log I(s), is plotted versus the scattering vector $s = 2 \sin \theta/\lambda$ (2θ = scattering angle, λ = wavelength = 0.15 nm), and the spacings d are calculated according to $s = 1/d$.

Fluorescence Resonance Energy Transfer Spectroscopy (*FRET*). Transport of the lipids into liposomes made from phosphatidylserine (PS) or a phospholipid mixture corresponding to that of the macrophage membrane PL_{M_ϕ}, mediated by lipopolysaccharide-binding protein (LBP), was determined by FRET spectroscopy applied as a probe dilution assay (*18*). To the liposomes, which were labeled with the donor dye NBD-phosphatidylethanolamine (NBD-PE) and acceptor dye Rhodamine-PE, first the lipids and then LBP were added, all at a final concentration of 1 μM. Intercalation was monitored as increase of the ratio of the donor intensity, I_D, at 531 nm to that of the acceptor intensity, I_A, at 593 nm in dependence on time.

Stimulation of Mononuclear Cells (MNC) by the Lipids. Mononuclear cells (MNC) were isolated from heparinized blood of healthy donors as described previously (*9*). The cells were resuspended in medium (RPMI 1640), and their number was adjusted to 5×10^6 cells/ml. For stimulation, 200 μL of MNC (1×10^6 cells) was transferred into each well of a

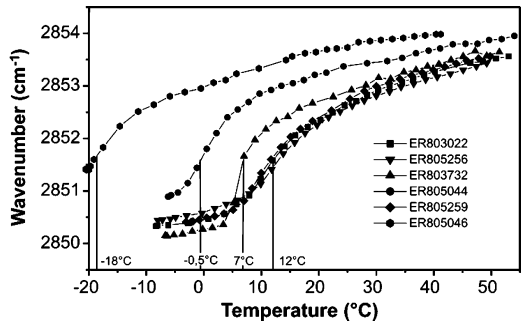

FIGURE 2: Gel to liquid crystalline phase transition behavior of the six ER compounds. The peak position of the symmetric stretching vibration of the methylene groups, $\nu_s(CH_2)$, is plotted versus temperature. Lipid concentration is 10 mM. In the gel phase, wavenumbers are observed between 2850.0 and 2850.5 cm^{-1} and in the liquid crystalline phase between 2852.5 and 2853.5 cm^{-1}.

96-well culture plate. The lipids were incubated for 30 min at 37 °C and added to the cultures at 20 μL per well. The cultures were incubated for 4 h at 37 °C under 5% CO_2. Supernatants were collected after centrifugation of the culture plates for 10 min at 400*g* and stored at −20 °C until determination of TNFα content. Immunological determination of TNF was carried out in a sandwich ELISA using a monoclonal antibody against TNF (clone 6b from Intex AG, Switzerland) and has been described earlier in detail (*19*).

Activation of CHO Reporter Cells. The CHO/CD14 reporter cell line, clone 3E10, is a stably transfected CD14-positive CHO (Chinese hamster ovary) cell line that expresses inducible membrane CD25 (Tac antigen) under transcriptional control of the human E-selectin promoter pELAM.Tac (*20*). The CHO reporter cell line EL1 (CD14-free) was obtained by stable cotransfection of CHO-K1 cells with the plasmid pCEP4 and pELAM.Tac and was a kind gift of Dr. Egil Lien. Both cell lines react sensitively to the activation of nuclear factor NF-κB.

RESULTS

Gel to Liquid Crystalline Phase Transition Behavior. The $\beta \leftrightarrow \alpha$ gel to liquid crystalline phase transition of the hydrocarbon chains was measured with infrared spectroscopy via the determination of the peak position of the symmetric stretching vibration of the methylene groups $\nu_s(CH_2)$. In Figure 2, the wavenumber values of the peak positions are plotted against temperature for all investigated ER compounds. Interestingly, among the stereoisomers ER803022, ER803732, ER805256, and ER805259, the compound with the acyl chain linkages in R,S,S,R-configuration (ER803732) has not only a significantly lower phase transition temperature, T_c (at approximately 7 °C), than the other samples (around 12 °C) but also a sharper transition. For the compounds with longer backbone spacer, T_c decreases drastically to −0.5 °C for ER805044 with $n = 4$ (see Figure 1) and to −18 °C for ER805046 with $n = 8$. The transition was also determined with DSC, which is shown exemplarily in Figure 3 for ER803022. The data show considerable increases of the phase transition enthalpy between the first and all further scans. Striking are the ΔH values of 7.9−15.9 kJ·mol^{-1}, which are thus considerably lower than those found for hexaacyl LPS (28−38 kJ·mol^{-1} (*21*, *22*)) and even for diacyl C14 phospholipids (25−30 kJ·mol^{-1} (*23*)).

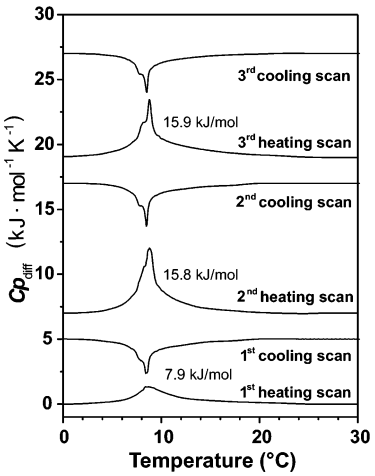

FIGURE 3: Differential scanning calorimetry data, plotted as the specific excess heat capacity c_p versus temperature T, of ER803022 for three subsequent heating and cooling scans. Lipid concentration is 1 mg/mL.

The first heating scan (Figure 3) represents the phase transition of a cold hydrated lipid from the gel phase into the liquid crystalline phase. The peak maximum of the phase transition is located at $T_c = 8.4$ °C ($T_{1/2} = 3.8$ °C) with a phase transition enthalpy of $\Delta H_c = +7.9$ kJ·mol^{-1}. The following cooling scan shows no hysteresis with respect to the heating scan ($T_c = 8.4$ °C with a shoulder at 7.8 °C and a $\Delta H_c = -7.5$ kJ·mol^{-1}) for the recrystallization of the fluid hydrocarbon chains into an ordered phase with the acyl chains mainly aligned in an all-trans conformation.

The second heating scan, however, represents the thermotropic phase behavior of a lipid hydrated in the liquid crystalline phase. By comparing the heat capacity curves of the first and the second heating scan, it becomes obvious that the thermotropic phase behavior depends on the hydration protocol. The maximum of the heat capacity of the second heating scan is $T_c = 8.8$ °C with a shoulder in the heat capacity curve at ∼8 °C and a $\Delta H_c = +15.8$ kJ·mol^{-1}. The higher phase transition enthalpy suggests that the presence of water in the polar interface region of the lipid after hydration in the liquid crystalline phase increases the van der Waals interactions between the acyl chains.

The phase transition enthalpy of the second cooling scan ($\Delta H_c = -7.4$ kJ·mol^{-1}) of ER803022 corresponds to that of the first cooling scan. The thermotropic parameters obtained from further heating and cooling cycles do not change with respect to those of the second cycle. The phase transition entropy $\Delta S_c = +56$ J·mol^{-1}·K^{-1} of hydrated ER803022 is also extremely low and similar to that obtained for the phospholipid dilauroyl phosphatidylethanolamine (DLPE, $n = 12{:}0$) (*24*).

For endotoxins, it has been reported that the phase transition behavior strongly depends on the presence of, in particular, divalent cations such as Mg^{2+} as well as on the water content (lyotropism) (*25*, *26*). Therefore, the influence of these parameters on the $\beta \leftrightarrow \alpha$ acyl chain melting of one particular compound, ER803022, was investigated. From Figure 4, it becomes obvious that T_c increases from 12 °C in the absence of Mg^{2+} to 17 °C at an equimolar content of Mg^{2+} (Figure 4a). A reduction of the water content from 80% to 50% has no influence on T_c, only a further reduction

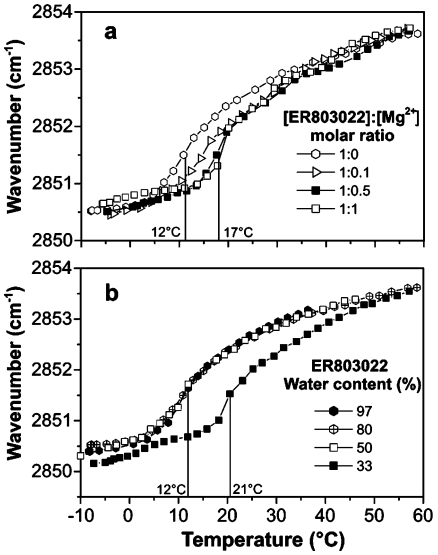

FIGURE 4: Gel to liquid crystalline phase transition behavior of ER803022 at different Mg^{2+} concentrations and at different water contents. Lipid concentration is 10 mM.

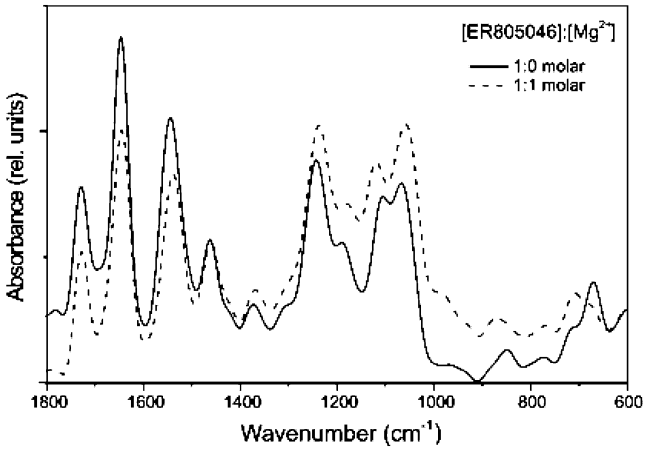

FIGURE 5: Infrared spectra of ER805046 in the range 1800−600 cm^{-1} in the absence and presence of an equimolar content of Mg^{2+} with an assignment of the bands to the different vibrational modes. The precise band positions are listed in Table 1. Lipid concentration is 1 mM.

to 33% causes a considerable increase of T_c from 12 to 21 °C (Figure 4b).

Molecular Groups. In Figure 5, infrared spectra are presented exemplarily for compound ER805046 in the wavenumber range 1800−600 cm^{-1} and in the absence and the presence of an equimolar amount of Mg^{2+}. The single peaks are assigned to the respective vibrations. Obviously, for many vibrational bands, the addition of Mg^{2+} leads to significant changes of the peak position.

A detailed determination of the individual peak positions in the absence and presence of Mg^{2+} is given in Table 1 for the three compounds ER803022, ER805259, and ER805046. In particular for the phosphate bands, the Mg^{2+}-induced shift is high. Interestingly, for $\nu_{as}(PO_2^-)$ Mg^{2+} causes a decrease, whereas for $\nu_s(PO_2^-)$ it causes a drastic increase of the wavenumber values.

Aggregate structures. Synchrotron radiation X-ray diffraction experiments are presented exemplarily for ER803022, ER805259, and ER805046 for different ambient conditions. The results at high water content at 20 °C in the absence of Mg^{2+} are given in Figure 6. The diffraction patterns of ER803022 and ER805259 indicate a complex superposition of different structures, a broad maximum between 0.1 and 0.4 nm^{-1}, corresponding to a unilamellar structure, and further peaks, which might be related to nonlamellar, probably cubic structures. In contrast, ER805046 exhibits only a broad maximum characteristic of a pure unilamellar phase or a multilamellar phase with low lamellarity. Experiments performed at higher temperatures up to 70 °C showed very similar diffraction patterns, that is, the same basic aggregate structures.

The results in the presence of equimolar concentration of Mg^{2+} are plotted in Figure 7. At 20 °C, all three samples exhibit diffraction maxima with equidistant spacing ratios typical for a multilamellar structure. This structure is maintained for ER805046 up to 70 °C. In contrast, for ER805259 and ER803022, the diffraction patterns change already at 50 °C to one main reflection and two further reflections at $1/\sqrt{3}$ and $1/\sqrt{4}$ of the main spacing. This pattern is characteristic for the inverted hexagonal phase, H_{II}. The results at a lower water concentration of 50% are presented in Figure 8 for ER805259 and ER803022. Clearly, the patterns for ER805259 are typical for a multilamellar structure at all temperatures, whereas those for ER803022 under these conditions demonstrate the existence of a nonlamellar cubic phase. For example, at 20 °C, the diffraction maxima at 3.88, 3.38, and 2.91 nm can be indexed as $1/\sqrt{8}$-, $1/\sqrt{10}$-, and $1/\sqrt{14}$-fold, respectively, of the periodicity $a_Q = 10.8 \pm 0.1$ nm. The two further reflections, however, cannot readily be assigned.

Summarized, the tendency of ER803022 to form nonlamellar structures is strong and that of ER805259 lower, whereas ER805046 displays no such tendency at all. From the aggregate structure, the shapes of the single molecules composing the aggregates can be deduced: ER803022 molecules have the strongest tendency to adopt a conical-concave conformation (the hydrophobic moiety has a higher cross-section than the hydrophilic), ER805259 molecules adopt a less conical conformation, and those of ER805046 adopt a purely cylindrical one.

The X-ray diffraction experiments gave for ER803732 a slight tendency toward a conical shape and for ER805044 an exclusively cylindrical shape (data not shown).

Intercalation into Target Cell Membranes. We have reported previously that a necessary step for cell activation is the intercalation of LPS into the phospholipid matrix of the target membranes mediated by lipopolysaccharide-binding protein (LBP). This intercalation of the ER compounds was tested with phospholipid liposomes as model membranes applying FRET spectroscopy (Figure 9). To this end, in a first step, the ER compounds, and for comparative purposes also LPS Re, were added to phosphatidylserine (PS) liposomes. This did not yield a significant change of the fluorescence signal except a slight intensity decrease due to the dilution. However, the addition of LBP in a second step after 100 s led to a strong intensity increase for all investigated samples. For the phospholipid mixture corresponding to the composition of the macrophage membrane, PL_{M_ϕ}, similar results were found, only the signals were less expressed.

Cytokine-Inducing Capacity. The cytokine (tumor-necrosis-factor α, interleukins) induction of mononuclear cells is an

Table 1: Assignment and Peak Positions (Wavenumbers in cm^{-1}) of Vibrational Bands from Three Selected ER Compounds in the Absence (Top Values) and Presence of Mg^{2+} (Bottom Values)[a]

	compound		
vibration	ER803022	ER805259	ER805046
ester carbonyl ν(C═O)	1730.3	1732.7	1729.1
	1732.0	1731.7	1727.3
amide I	1653.5	1651.9	1645.8
	1650.1	1651.0	1644.9
amide II	1556.6 and 1537.5	1558.1 and 1540.7	1544.2
	1558.4 and 1539.2	1558.1 and 1539.9	1539.0
δ (CH_2)	1463.3	1461.8	1462.6
	1459.0	1461.8	1460.9
δ_s(CH_3)	1372.5	1375.5	1372.2
	1372.9	1372.2	1368.9
phosphate	1237.9	1239.8	1243.0
ν_{as}(PO_2^-)	1230.8	1231.2	1237.6
ester (C−O)	1183.8	1184.5	1184.4
	1176.8	1179.0	1176.8
phosphate	1107.0	1106.3	1110.6
ν_s(PO_2^-)	1119.1	1116.1	1119.3
−C−O−P−O−C−	1059.9	1060.7	1066.1
	1054.0	1051.0	1057.5
na	833.3	835.1	848.1
		(840.3) weak	868.3
na	664.5	667.8	670.4
	668.4	667.8	709−4 (double peaks)

[a] ν = stretching, δ = bending vibrations; s = symmetric, as = antisymmetric vibrations; na = not assignable.

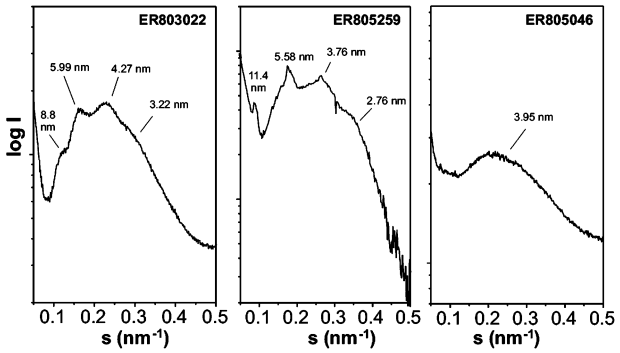

FIGURE 6: Synchrotron radiation X-ray diffraction patterns of three selected ER compounds at 90% water content. Lipid concentration is 50 mM. The numbers indicate the spacings $d = 1/s$. Due to this nonlinear scale, the precision of the peak determination is different. For example, the precision of the peak at 3.22 nm (left-hand figure) is ±0.01 nm; that at 8.8 nm is ±0.1 nm. The diffraction peak at 3.95 nm (right-hand figure) indicates the center of the broad reflection.

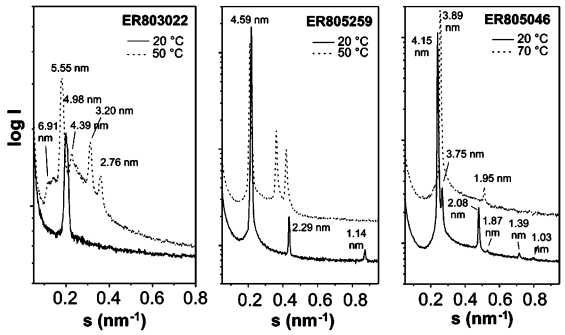

FIGURE 7: Synchrotron radiation X-ray diffraction patterns of three selected ER compounds at 80% water content in the presence of an equimolar amount of Mg^{2+} and at two temperatures. The logarithm of the scattering intensity, log $I(s)$, is plotted versus the scattering vector $s = 2 \sin \theta/\lambda$; 2θ = scattering angle, λ = wavelength = 0.15 nm.

endotoxin-typical biological action. Therefore, the capacity of the ER compounds to induce TNFα was tested with human mononuclear cells (MNC). The results presented in Figure 10 show that the capacity was highest for ER803022 and comparable to that of LPS Re (ref *9*, not shown). The three compounds with the same chemical structure but stereochemical changes in acyl chain branching (see Figure 1) have medium (ER805256, ER805259) or weak (ER803732) TNFα-inducing capacity, and the compounds with a larger backbone have very low ($n = 4$, ER805044) or even no ($n = 8$, ER805046) TNFα-inducing capacity.

CHO Cell Reporter System. To investigate a possible involvement of CD14 and TLR4 in the recognition of the ER compounds, their activity was investigated in a Chinese hamster ovary (CHO) cell reporter system and compared with interleukin-1 (IL-1) as a standard. These cells are natural TLR2 knockouts and express the human CD25 surface antigen upon induction of NF-κB translocation. The experiments with the EL1 (only TLR4 is expressed) and 3E10 (CD14 + TLR4) cells indicate that TLR4 alone is sufficient to respond to ER803022, but not to ER805046 (data not shown). In further experiments, the reactivity of 3E10 cells additionally transfected with human TRL2 were analyzed (Figure 11). Clearly, the inactive compound ER805046 did not activate the expression of CD25. However, it is noteworthy that the compounds with very low TNFα-inducing capacity (ER805044 and ER803732, see Figure 9) activate the expression of CD25 to a level comparable to that of the active compounds ER803022, ER805256, and ER805259.

For all ER compounds, the cells transfected with TLR2 react less, indicating that this receptor does not play a role in the signaling process.

DISCUSSION

The observed correlation between the biological activity and the physicochemical characteristics of the ER compounds

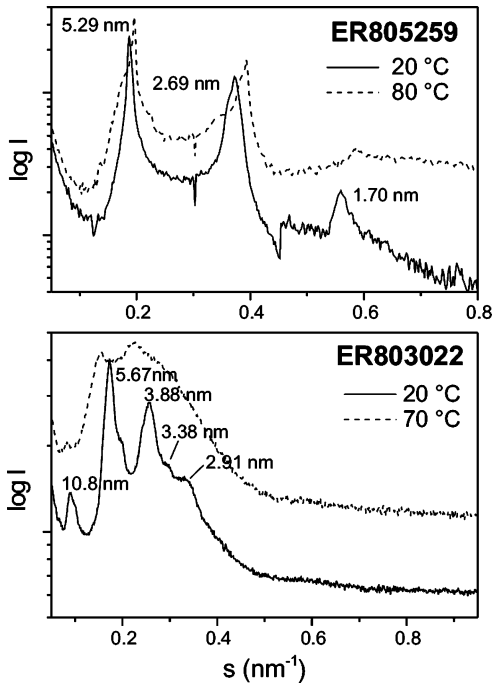

FIGURE 8: Synchrotron radiation X-ray diffraction patterns of ER805259 and ER803022 at 50% water content and two temperatures. Lipid concentration is 50 mM. The logarithm of the scattering intensity, log $I(s)$, is plotted versus the scattering vector $s = 2 \sin \theta/\lambda$.

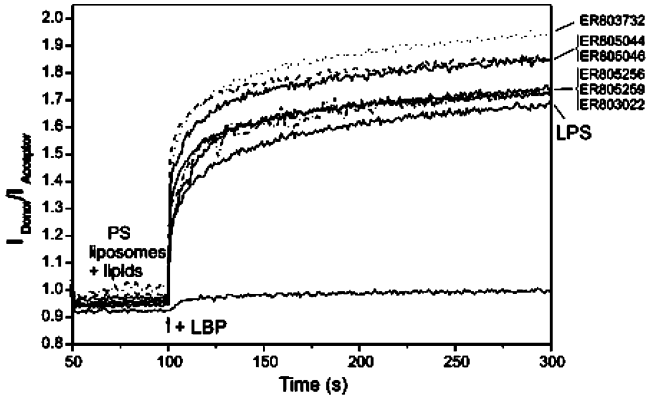

FIGURE 9: Time dependence of the ratio of donor fluorescence intensity, I_D, at 531 nm to that of the acceptor fluorescence intensity, I_A, at 593 nm for the six ER compounds as compared to lipopolysaccharide LPS Re from *Salmonella minnesota* strain R595. The lipids were added to the phosphatidylserine (PS) liposomes at 50 s, and LBP was added after 100 s. The final concentration of all compounds was 1 μM.

follow similar rules as that described earlier for endotoxins (*4*, *7*, *9*). The presented interpretation can be deduced from the preference of the compounds to adopt cubic inverted structures (Figures 6−8), from their ability to intercalate into phospholipid liposomes in the presence of LBP (Figure 9), and from their capacity to induce cytokines (Figure 10). Additionally, other endotoxin-typical characteristics are shared by the synthetic compounds: the presence of Mg^{2+} (Figure 4a) and a decrease of the water concentration (Figure 4b) cause an increase in the gel to liquid crystalline phase transition temperature, T_c, thus mimicking the properties for endotoxins (*25*, *26*), although the absolute values of T_c of the ER compounds (Figure 2) do not compare with those of enterobacterial endotoxins (LPS, 30−37 °C; lipid A, 40−45 °C (*21*, *25*)). However, the lyotropism, that is, the increase

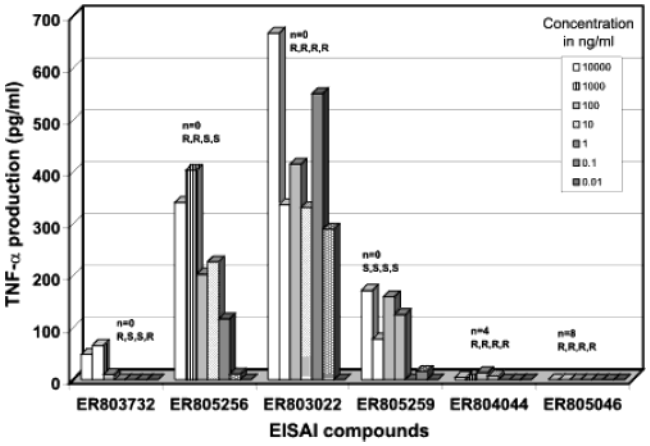

FIGURE 10: Production of tumor necrosis factor α (TNFα) from human mononuclear cells in dependence on concentration for the six ER compounds.

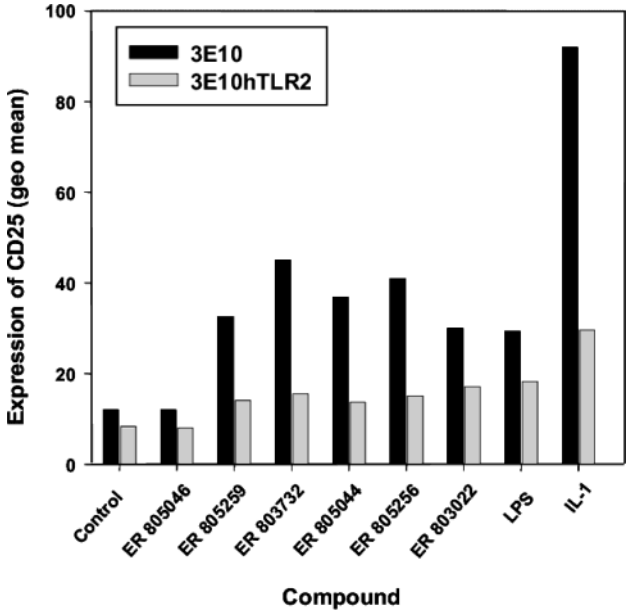

FIGURE 11: Relative activation of CHO reporter cells stimulated by the six ER compounds in comparison to LPS Re from *Salmonella minnesota* strain R595 and IL-1 as standard. The 3E10 cell line expresses CD14 and hamster TLR4, and the 3E10hTLR2 cell line additionally expresses human TLR2.

of T_c when lowering the water content, for the ER compounds is only observed at water contents significantly below 50% (Figure 4b), while for endotoxins it occurs already when lowering the water content from 90% to 60−70% (*27*). A possible explanation of this different behavior may be the presence of the sugar backbone in endotoxins, which can bind a significantly higher amount of water molecules than the serine-like backbone of the ER compounds.

Interestingly, the phase transition data allow a discrimination between active and inactive compounds. As illustrated in Figure 2, the three highly active compounds ER803022, ER805256, and ER805259 have an identical phase behavior, while the other less active compounds melt at significantly lower T_c.

Also, the influence of the stereochemistry becomes evident. For all compounds with the shortest backbone ($n = 0$, Figure 1), only the R,S,S,R configuration of ER803732 leads to a change in T_c (from 12 to 7 °C). Moreover, the insertion of the backbone spacer ($n = 8$, ER805046) leads not only to a

drastic decrease in T_c to −18 °C and increase in the wavenumbers of $\nu_s(CH_2)$ over the whole temperature range, reflecting a much less dense acyl chain packing than for the compounds with short backbone, but also to interesting dependences of the peak positions of the infrared vibrational bands. For example, for the different compounds, dramatic changes of the wavenumbers in particular for the three bands originating from the phosphates but also for the amide bands can be observed (Figure 5, Table 1). In this context also the low value of the enthalpy change ΔH_c (approximately 16 kJ·mol^{-1} as compared to 30−35 kJ·mol^{-1} for LPS) should be mentioned. This reduction may be assumed to be due to the particular chemical structure of the ER compounds with hydrophilic amide and ester groups deeply penetrating the hydrophobic moiety thus leading to a much more unfavorable acyl chain packing as in the case of LPS.

The presented X-ray diffraction data (Figures 6−8) allow a quantitative description of the endotoxin action of the compounds: whereas the biologically completely inactive ER805046 forms a lamellar phase under all conditions (unilamellar at 90% water content, Figure 6; multilamellar at 80% in 100 mM Mg^{2+} at 20 °C as well as 70 °C, Figure 7), the aggregate structures of the active compounds can be characterized according to their degree of activity. ER803022, the compound with highest bioactivity has the strongest tendency to form inverted structures, adopting a nonlamellar cubic structure even at 50% water content, where the less active compound ER805259 exhibits already a multilamellar characteristic (Figure 8). Thus, the propensity of a given compound to adopt nonlamellar structures seems to be directly correlated with the ability to induce cytokine production in immune cells.

The presented data allow us to conclude that the determination of the aggregate structure under near physiological conditions as shown in Figure 6 may be sufficient to differentiate between completely active and inactive compounds. It must be conceded, however, that a differentiation between active compounds with different degrees of activity is not as easy. In this case, variation of ambient conditions such as water and Mg^{2+} content (Figures 7 and 8) is necessary for a quantitative discrimination. These data may be important in the light of our mechanistic interpretation of endotoxin action as described below.

Expression of TLR4 alone is sufficient to enable the cells to respond to the highly active compound ER803022, deduced from the results of the CHO reporter cell system indicating that the coexpression of CD14 does not change the picture (Figure 11). In contrast, neither the cells expressing TLR4 alone nor those coexpressing TRL4 and CD14 respond to inactive ER805046. The results for the compounds with medium to high activity, ER805256 and ER805259 (Figure 10), show the expected reactivity. However, surprisingly, the cells also respond to the compounds exhibiting very low activity (ER803732 and ER805044). These data suggest that the cell surface receptor TLR4 alone may not be necessarily sufficient for cell activation.

The presented results strongly support our model of endotoxin action: the interaction of endotoxin with LBP and soluble and membrane-bound CD14 leads to an intercalation of the endotoxins into the membrane of immune cells, in which they may laterally diffuse to the sites of signaling proteins such as the Toll-like receptors (*28*, *29*) or the K^+ channel MaxiK (*30*). The latter has been shown to be involved in transmembrane signaling by various bacterial virulence factors in a very early step. Agonistically active endotoxins, with a conical shape of the lipid A moiety, may exert a sterical stress after intercalation into the membrane, which may then induce a conformational change of the receptor proteins leading to cell activation. Agonistically inactive compounds are not able to cause a conformational change, but they may occupy the LPS binding sites of the proteins and therefore block agonistic action. It should be emphasized that this "conformational concept" may well contribute to an understanding of cell activation; however, an absolute proof for the occurrence of the single steps such as membrane binding to signaling proteins is still lacking. In this context, we would like to suggest that membrane activity of biologically relevant compounds might be a process of general importance. Thus, for example, Navab et al. (*31*) observed for particular peptides with different hydrophobicity variations in their association with membrane phospholipids, which again strongly influenced inflammation processes.

As described, the main physical−chemical characteristics of the synthesized phospholipids compare well with those of bacterial endotoxins, and the same is true for a typical endotoxic reaction, the cytokine induction in mononuclear cells. Additionally, we have shown that the specific MaxiK channel blocker, paxilline, which is able to inhibit the endotoxin-induced cytokine production (*30*), is also able to block that of the ER803022 compound (*9*).

In conclusion, we have shown that amphiphilic lipid molecules such as the ER compounds with clearly separated hydrophilic and hydrophobic moieties, with at least two negative charges in the headgroup, and with the preference to adopt nonlamellar inverted (cubic, H_{II}) aggregate structures exhibit a strong capacity to activate mononuclear cells and that for cell activation a general mechanism according to the mechanistic principle described above may be valid.

ACKNOWLEDGMENT

We thank G. von Busse, C. Hamann, and U. Diemer for performing the FTIR- and FRET-spectroscopic and LAL measurements, respectively, E. Lien for providing the EL1 CHO reporter cell line, and S. F. Carroll for the kind gift of LBP. B. Fölting and C. Hillmann are acknowledged for excellent technical assistance.

REFERENCES

1. Rietschel, E. T., Brade, H., Holst, O., Brade, L., Müller-Loennies, S., Mamat, U., Zähringer, U., Beckmann, F., Seydel, U., Brandenburg, K., Ulmer, A. J., Mattern, T., Heine, H., Schletter, J., Hauschildt, S., Loppnow, H., Schönbeck, U., Flad, H.-D., Schade, U. F., di Padova, F., Kusumoto, S., and Schumann, R. R. (1996) Bacterial endotoxin: Chemical constitution, biological recognition, host response, and immunological detoxification, *Curr. Top. Microbiol. Immunol. 216*, 39−80.
2. Zähringer, U., Lindner, B., and Rietschel, E. T. (1994) Molecular structure of lipid A, the endotoxic center of bacterial lipopolysaccharides, *Adv. Carbohydr. Chem. Biochem. 50*, 211−276.
3. Loppnow, H., Brade, H., Dürrbaum, I., Dinarello, C. A., Kusumoto, S., Rietschel, E. T., and Flad, H.-D. (1989) IL-1 induction-capacity of defined lipopolysaccharide partial structures, *J. Immunol. 142*, 3229−3238.
4. Schromm, A. B., Brandenburg, K., Loppnow, H., Moran, A. P., Koch, M. H. J., Rietschel, E. T., and Seydel, U. (2000) Biological

activities of lipopolysaccharides are determined by the shape of their lipid A portion, *Eur. J. Biochem. 267*, 2008−2013.
5. Kovach, N. L., Yee, E., Munford, R. S., Raetz, C. R. H., and Harlan, J. M. (1990) Lipid IVa inhibits synthesis and release of tumor necrosis factor induced by lipopolysaccharide in human whole blood ex vivo, *J. Exp. Med. 172*, 77−84.
6. Loppnow, H., Rietschel, E. T., Brade, H., Schönbeck, U., Libby, P., Wang, M.-H., Heiner, H., Feist, W., Dürrbaum-Landmann, I., Ernst, M., Brandt, E., Grage-Griebenow, E., Ulmer, A. J., Campos-Portuguez, S., Schade, U., Kirikae, T., Kusumoto, S., Krauss, J., Mayer, H., and Flad, H.-D. (1993) Lipid A precursor Ia (compound 406) and *Rhodobacter capsulatus* lipopolysaccharide: potent endotoxin antagonists in the human system in vitro, in *Bacterial endotoxin: Recognition and effector mechanisms* (Levin, J., Alving, C. R., Munford, R. S. and Stütz, P., Eds.), pp 337−348, Elsevier, Amsterdam.
7. Brandenburg, K., Andrä, J, Müller, M., Koch, M. H. J., and Garidel, P. (2003) Physicochemical properties of bacterial glycopolymers in relation to bioactivity, *Carbohydr. Res. 338*, 2477−2489.
8. Müller, M., Scheel, O., Lindner, B., Gutsmann, T., and Seydel, U. (2003) The role of membrane-bound LBP, endotoxin aggregates, and the MaxiK channel in LPS-induced cell activation, *J. Endotoxin Res. 9*, 181−186.
9. Seydel, U., Hawkins, L., Schromm, A. B., Heine, H., Scheel, O., Koch, M. H. J., and Brandenburg, K. (2003) The generalized endotoxic principle, *Eur. J. Immunol. 33*, 1586−1592.
10. Takada, H., Kotani, S., Tanaka, S., Ogawa, T., Takahashi, I., Tsujimoto, M., Komuro, T., Shiba, T., Kusumoto, S., and Kusunose, N. (1988) Structural requirements of lipid A species in activation of clotting enzymes from the horseshoe crab, and the human complement cascade, *Eur. J. Biochem. 175*, 573−580.
11. Krisovitch, S. M., and Regen, S. L. (1992) Nearest neighbor recognition in phospholipid membrane: a molecular-level approach to the study of membrane suprastructure, *J. Am. Chem. Soc. 114*, 9828−9835.
12. Hawkins, L. D., Ishizaka, S. T., Lewis, M., McGuiness, P., Nault, A., Rose, J., and Rossignol, D. (2001) Immunological adjuvant compounds, compositions, and methods of use thereof, U.S. Patent, 6,290,973 B1.
13. Blume, A., and Garidel P. (1999). Lipid model membranes and biomembranes, in *From Macromolecules to Man* (Gallagher, P. K. series Ed., Kemp, R. B., Ed.), The Handbook of Thermal Analysis and Calorimetry, 1st ed., Vol. 4, pp 109−173, Elsevier, Amsterdam.
14. Garidel, P., Johann, C., and Blume, A. (2000) Thermodynamics of lipid organization and domain formation in phospholipid bilayers, *J. Liposome Res. 10*, 131−158.
15. Koch, M. H. J., and Bordas, J. (1983) X-ray diffraction and scattering on disordered systems using synchrotron radiation, *Nucl. Instrum. Methods 208*, 461−469.
16. Gabriel, A. (1977) Position-sensitive X-ray detector, *Rev. Sci. Instrum. 208*, 1303−1305.
17. Brandenburg, K., Richter, W., Koch, M. H. J., Meyer, H. W., and Seydel, U. (1998) Characterization of the nonlamellar cubic and H_{II} structures of lipid A from *Salmonella enterica* serovar Minnesota by X-ray diffraction and freeze-fracture electron microscopy, *Chem. Phys. Lipids 91*, 53−69.
18. Gutsmann, T., Schromm, A. B., Koch, M. H. J., Kusumoto, S., Fukase, K., Oikawa, M., Seydel, U., and Brandenburg, K. (2000) Lipopolysaccharide-binding protein-mediated interaction of lipid A from different origin with phospholipid membranes, *Phys. Chem. Chem. Phys. 2*, 4521−4528.
19. Gallati, H. (1982) Interferon: Wesentlich vereinfachte, enzymimmunologische Bestimmung mit zwei monoklonalen Antikörpern, *J. Clin. Chem. Clin. Biochem. 20*, 907−914.
20. Delude, R. L., Yoshimura, A., Ingalls, R. R., and Golenbock, D. T. (1998) Construction of a lipopolysaccharide reporter cell line and its use in identifying mutants defective in endotoxin, but not TNF-α, signal transduction, *J. Immunol. 161*, 3001−3009.
21. Brandenburg, K., and Seydel, U. (1984) Physical aspects of structure and function of membranes made from lipopolysaccharides and free lipid A, *Biochim. Biophys. Acta 775*, 225−238.
22. Brandenburg, K., Jürgens, G., Andrä, J., Lindner, B., Koch, M. H. J., Blume, A., and Garidel, P. (2002) Biophysical characterization of the interaction of high-density lipoprotein (HDL) with endotoxins, *Eur. J. Biochem. 269*, 5972−5981.
23. Silvius, J. R. (1982) Thermotropic phase transitions of pure lipids in model membranes and their modification by membrane proteins, *Lipid−Protein Interact. 2*, 239−281.
24. Blume, A. (1991) Biological calorimetry: Membranes, *Thermochim. Acta 193*, 299−347.
25. Brandenburg, K., Koch, M. H. J., and Seydel, U. (1990) Phase diagram of lipid A from *Salmonella minnesota* and *Escherichia coli* rough mutant lipopolysaccharide, *J. Struct. Biol. 105*, 11−21.
26. Brandenburg, K., Koch, M. H. J., and Seydel, U. (1992) Phase diagram of deep rough mutant lipopolysaccharide from *Salmonella minnesota* R595, *J. Struct. Biol. 108*, 93−106.
27. Brandenburg, K., and Seydel, U. (1990) Investigation into the fluidity of lipopolysaccharide and free lipid A membrane systems by Fourier-transform infrared spectroscopy and differential scanninig calorimetry, *Eur. J. Biochem. 191*, 229−236.
28. Chow, J. C., Young, D. W., Golenbock, D. T., Christ, W. J., and Gusovsky, F. (1999) Toll-like receptor-4 mediates lipopolysaccharide-induced signal transduction, *J. Biol. Chem. 274*, 10689−10692.
29. Anderson, K. V. (2000) Toll signaling pathways in the innate immune response, *Curr. Opin. Immunol. 12*, 13−19.
30. Blunck, R., Scheel, O., Müller, M., Brandenburg, K., Seitzer, U., and Seydel, U. (2001) New insights into endotoxin-induced activation of macrophages: Involvement of a K^+ channel in transmembrane signalling, *J. Immunol. 166*, 1009−1015.
31. Navab, M., Anantharamaiah, G. M., Reddy, S. T., Van Lentan, B. J., Hough, G., Wagner, A., Nakamura, K., Garber, D. W., Datta, G., Segrest, J. P., Hama, S., and Fogelman, A. M. (2003) Human apolipoprotein AI mimetic peptides for the treatment of atherosclerosis, *Curr. Opin. Invest. Drugs 4*, 1100−1104.

BI0361158